Hindawi Publishing Corporation
Mathematical Problems in Engineering
Volume 2014, Article ID 295320, 12 pages
http://dx.doi.org/10.1155/2014/295320

Research Article

Active Contour Model for Ultrasound Images with Rayleigh Distribution

Guodong Wang,[1] Qian Dong,[2] Zhenkuan Pan,[1] Ximei Zhao,[1] Jinbao Yang,[1] and Cunliang Liu[1]

[1] *College of Information Engineering, Qingdao University, Qingdao 266071, China*
[2] *The Affiliated Hospital of Medical College, Qingdao University, Qingdao 266003, China*

Correspondence should be addressed to Guodong Wang; doctorwgd@gmail.com

Received 9 February 2014; Revised 3 June 2014; Accepted 5 June 2014; Published 29 June 2014

Academic Editor: Wanquan Liu

Ultrasound images are often corrupted by multiplicative noises with Rayleigh distribution. The noises are strong and often called speckle noise, so segmentation is a hard work with this kind of noises. In this paper, we incorporate multiplicative noise removing model into active contour model for ultrasound images segmentation. To model gray level behavior of ultrasound images, the classic Rayleigh probability distribution is considered. Our model can segment the noisy ultrasound images very well. Finally, a fast method called Split-Bregman method is used for the easy implementation of segmentation. Experiments on a variety of synthetic and real ultrasound images validate the performance of our method.

1. Introduction

Ultrasound imaging is a cheap and convenient technique in clinical diagnosis. However, the ultrasound image is often suffering from speckle noise. The noise is strong and often hinders diagnosis. Many authors model the speckle noise as multiplicative one with Rayleigh distribution. Ultrasound image segmentation is often considered a hard work because of the existence of the speckle noise. In this paper, we propose a new ultrasound image segmentation method using active contour model. Because the speckle noise is strong, we consider using an image restoration model for speckle noise removal as the fidelity term.

Most active contour models use edge detectors for assisting segmentation; however, clear boundaries between two areas with large noise are hard to be detected. These models need additional smoothing operation which will blur the edges. There are many traditional active contours based on an edge detection function for the stopping criteria [1–8]. However, this kind of active contour models has failed in many applications such as in medical images where fuzzy edges can be encountered. Besides, edge-based active contours are very sensitive to noise and initial position. Then active contour models based on region statistics information have been proposed. The statistics information contains mean value, variance, probability density function (pdf), and so on. Chan and Vese [9] proposed famous CV model for two-phase segmentation based on the mean values of different areas. The contour will stop at the position when the difference of mean values inside and outside the contour gets minimized. From then on, active contour models based on region information are proposed. Segmentation method based on statistical moments [10] is proposed for segmentation. Zhu and Yuille [11], Paragios and Deriche [12], and Rousson and Deriche [13] proposed using pdf descriptor which can be modeled by using mixture of Gaussians for segmentation. Herbulot et al. [14], Jehan-Besson et al. [15], and Aubert et al. [16] proposed using shape gradient-based joint intensity distribution. In these models, the pdf of different areas is updated in every step of iteration until the optimal partition is reached. Liu et al. [17] use the difference of probability density among different areas for segmentation. Yuan [18] proposes an active

contour model driven by local divergence energies for the segmentation. Pan et al. [19] proposed a geodesic active contour model based on global variables difference. The model can deal with medical images with strong contrast, complex topological structure, and low noise characteristics.

The segmentation methods mentioned above belong to the catalog of local minimization model which means that the quality of segmentation depends on the initial location of active contour. Bresson et al. [20] and Chan et al. [21] modified the classic CV model as a convex one which is called convex CV model. In these methods, the segmentation results are not affected by the initial condition. Besides, dual method and the splitting technique are adapted for the fast minimization with TV norm in [20]. Recently, the fast Split-Bregman method [22] is also applied to solve the convex active contour model and proved faster than dual method. The Split-Bregman method has several advantages. It is superior over graph cut in efficiency, accuracy, and memory requirement. It is actually equivalent to the augmented Lagrangian method [23, 24]. In this paper, we also design the Split-Bregman method for the easy implementation of our proposed new segmentation model.

All the methods mentioned above almost use the statistical information of different areas. However, the speckle noise is very strong in ultrasound images; statistical methods do not always get good performance. So, in this paper, we consider incorporating multiplicative noise removal model into active contour model for ultrasound image segmentation. Because the multiplicative noise removal model and the active contour model are iterated in a relatively independent manner, our method can get the real results without the influence of noise. In our previous work [25], we have proposed a model for images with Rayleigh distribution but the smoothing term we used is total variation. Wang et al. [26] have proved that noise removal for images corrupted by noise of Rayleigh distribution by using Perona-Malik term is superior to by using total variation. So, in this paper we proposed a new active contour model coupling with multiplicative noise removal model by using Perona-Malik term. During the iteration process, the noise removal model can reduce the effect of noise and the active contour model can get the real position of the interesting area. The proposed active contour model does not use edge detection method and this property enables our model to segment medical images without clear gradient boundaries. It is an improvement model on the piecewise-constant Mumford-Shah segmentation model [27].

The main contribution of the paper is as follows. First, we propose a new active contour model incorporated with ultrasound noise removing method. The novelty of the new model is that the proposed one does not do segmentation after noise removal; instead, these two processes are coupled together. Second, for easy implementation, the Split-Bregman method is designed for solving the model.

The outline of the paper is as follows. In the next section we introduce some multiplicative removing models. In Section 3 we propose our new active contour model for ultrasound images with multiplicative noise. Then we design the Split-Bregman methods for the easy implementation of the model. In Section 4, we test the proposed method on a variety of synthetic and real ultrasound images. The last section is conclusion.

2. The Multiplicative Noise Removing Models

In recent years, much attention was attracted to multiplicative noise removal. Many methods were proposed for multiplicative noise removal by using variational method [28–31]. RLO method [28] is the first variational method for multiplicative noise removal by using TV (total variation) method. AA model [29] is established by using maximum a posteriori (MAP) estimator. The energy function has proved that the minimum corresponds to the denoised image. Huang et al. [30] incorporate the modified total variation regularization in the objective function to recover image edges. The proposed model is a strictly convex objective function for multiplicative noise removal problems. Durand et al. [31] enhance the multiplicative noise removal ability by using L1 fidelity. Setzer et al. [32] proposed a variational method for multiplicative noise with Poissonian distribution by MAP method. Shi and Osher [33] proposed a convex model of multiplicative noise removal by using nonlinear inverse scale space. Shen [34] modified the TV model by dividing the gray value and called the modified one a Weberized TV model for multiplicative noise removal. Denis et al. [35] proposed a model for ultrasound noise removal with Rayleigh distribution using MAP. The model is very effective and we will incorporate it in our model.

The relative model function of [35] is shown in the following:

$$\min_{u} \left\{ \lambda \int_{\Omega} |\nabla u| \, dx \, dy + \int_{\Omega} \left(\frac{1}{2} \left(\frac{f}{u} \right)^2 + \log u \right) dx \, dy \right\}, \tag{1}$$

where f is the original noisy image, u is the denoised image we want, and λ is the balance parameter. We refer the reader to [35] for the derivation of this fidelity term using Bayesian statistics. In the next section, we will couple the above model with active contour model for ultrasound image segmentation.

3. Active Contour Model Coupling Multiplicative Noise Removing

The models for images segmentation corrupted by multiplicative noise with Rayleigh are not well developed. In [36], the authors proposed a model for multiplicative noise images segmentation, but from the model we find that it is a model fit for images with Gaussian distribution. In [37], the authors use variance information for segmentation introduced by MAP of Rayleigh distribution. The method does not consider the trait of multiplicative noise. So it is not fit for multiplicative noise very well.

To overcome the drawback of segmentation for images corrupted by multiplicative noise with Rayleigh distribution,

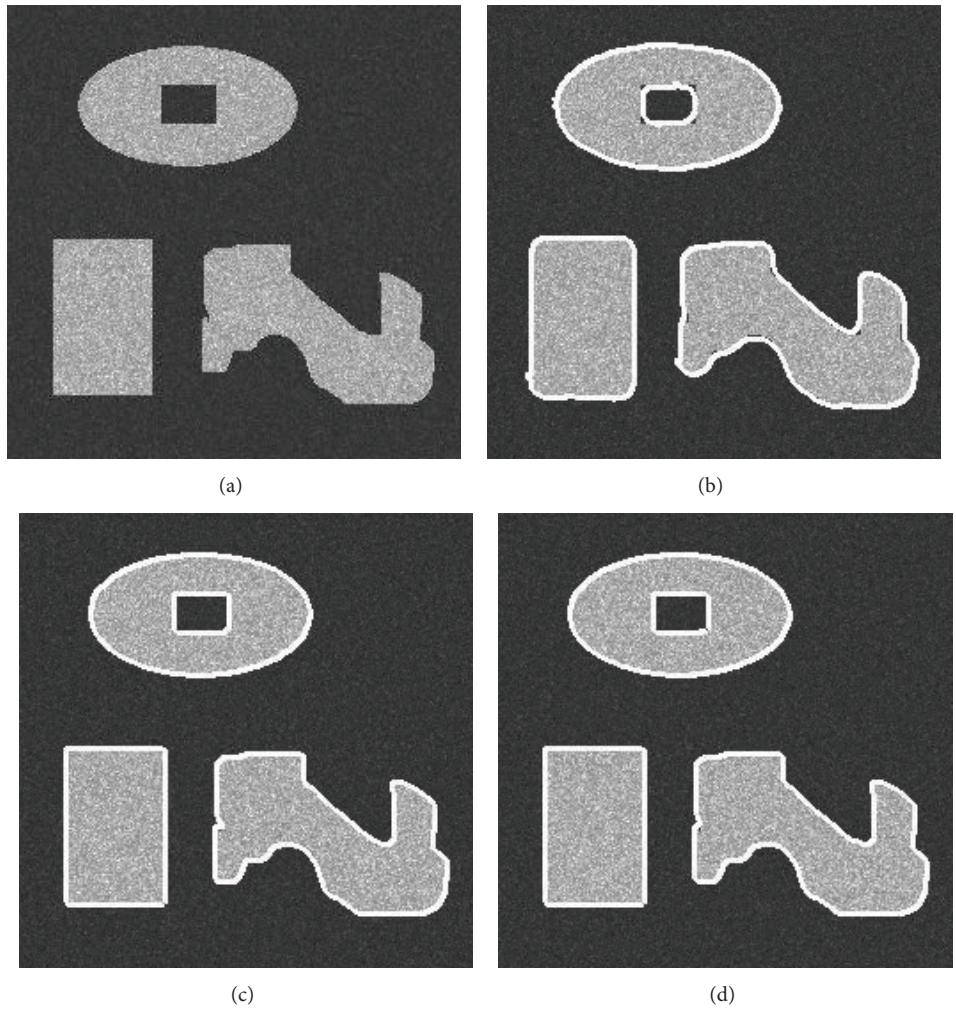

(a) (b) (c) (d)

Figure 1: Synthetic image corrupted by multiplicative noise with Rayleigh distribution for segmentation. (a) Original noised image. (b) The segmentation result using [36]. (c) The segmentation result using [37]. (d) The segmentation result using our proposed model.

the proposed new active contour model coupling with image denoising is

$$\begin{aligned}\arg\min_{\phi\in[0,1]} \Bigg\{ & \int_\Omega |\nabla\phi|\,dx\,dy \\ & + \int_\Omega \Bigg(\Bigg(\alpha_1 \left(\frac{1}{2}\left(\frac{f}{u_1}\right)^2 + \log u_1 \right) \\ & \quad + \beta_1 \varphi\left(|\nabla u_1|\right) \Bigg) \phi \\ & \quad + \left(\alpha_2 \left(\frac{1}{2}\left(\frac{f}{u_2}\right)^2 + \log u_2 \right) \right. \\ & \quad \left. + \beta_2 \varphi\left(|\nabla u_2|\right) \right) \\ & \quad \times (1-\phi) \Bigg) dx\,dy \Bigg\}, \end{aligned} \tag{2}$$

where Ω is the image domain, α_1, β_1, α_2, β_2 are the positive parameters, ϕ is a standard level set function and $\varphi(|x|) = \gamma^2 \ln(1 + (|x|^2/\gamma^2))$, and φ is the nonlinear diffusion function which can deal with noise very well. This is a global segmentation minimization problem due to convex set $\phi \in [0, 1]$. Chan et al. [21] transformed the original active contour model to a convex minimization problem by relaxing $\phi \in \{0, 1\}$ to $\phi \in [0, 1]$ and showed that the characteristic function is the global minimizer. Authors can refer to [21] for the details of algorithm implementation and the globally convex effects.

We modified the original active contour model as the form of (2) mainly because the gray values in different areas are not always the same. We replace the fidelity term $|f - u|^2$ of VC model with $\int_\Omega ((1/2)(f/u)^2 + \log u)dx$, so our model can segment images with multiplicative noise of Rayleigh distribution. This is a natural extension of CV [9] and VC [38] model for piecewise constant or smooth model. Because of the change of fidelity term, our model also encompasses pre-Rayleigh and post-Rayleigh distributions which occur in real ultrasound images.

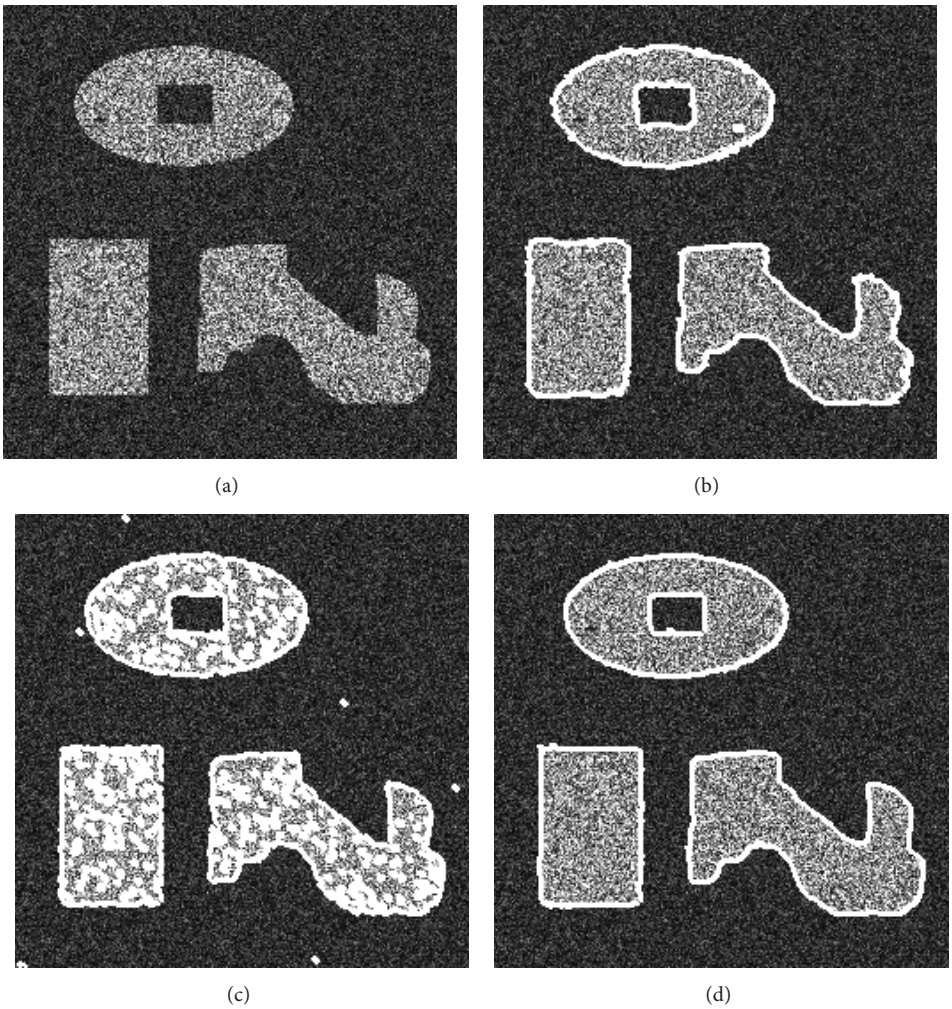

(a) (b) (c) (d)

Figure 2: Synthetic image corrupted by multiplicative noise with Rayleigh distribution for segmentation. (a) Original real ultrasound image. (b) The segmentation result using [36]. (c) The segmentation result using [37]. (d) The segmentation result using our proposed model.

Equation (2) can be divided into the following three subproblems of minimization:

$$\min_{u_1}\left\{E(u_1)=\int_\Omega\left(\alpha_1\left(\frac{1}{2}\left(\frac{f}{u_1}\right)^2+\log u_1\right)+\beta_1\varphi\left(\left|\nabla u_1\right|\right)\right)\phi\,dx\,dy\right\}, \tag{3}$$

$$\min_{u_2}\left\{E(u_2)=\int_\Omega\left(\alpha_2\left(\frac{1}{2}\left(\frac{f}{u_2}\right)^2+\log u_2\right)+\beta_2\varphi\left(\left|\nabla u_2\right|\right)\right)(1-\phi)\,dx\,dy\right\}, \tag{4}$$

$$\arg\min_{\phi\in[0,1]}\left\{E(\phi)=\int_\Omega\left|\nabla\phi\right|dx\,dy+\int_\Omega R(u_1,u_2)\,\phi\,dx\,dy\right\}, \tag{5}$$

where

$$R(u_1,u_2)=\left(\alpha_1\left(\frac{1}{2}\left(\frac{f}{u_1}\right)^2+\log u_1\right)+\beta_1\varphi\left(\left|\nabla u_1\right|\right)\right)\phi-\left(\alpha_2\left(\frac{1}{2}\left(\frac{f}{u_2}\right)^2+\log u_2\right)+\beta_2\varphi\left(\left|\nabla u_2\right|\right)\right)\phi. \tag{6}$$

In the following, we will solve (3), (4), and (5) by using the Split-Bregman method [23].

For solving (3), we introduce auxiliary vector variable $\overrightarrow{\omega}_1$ and Bregman iterative parameter $\vec{b}_1$ and transform (3) into the following equivalent minimization problems:

$$\vec{b}_1^{k+1}=\vec{b}_1^{k}+\nabla u_1^{k}-\vec{\omega}_1^{k},$$

$$\left(u_1^{k+1},\overrightarrow{\omega}_1^{k+1}\right)$$

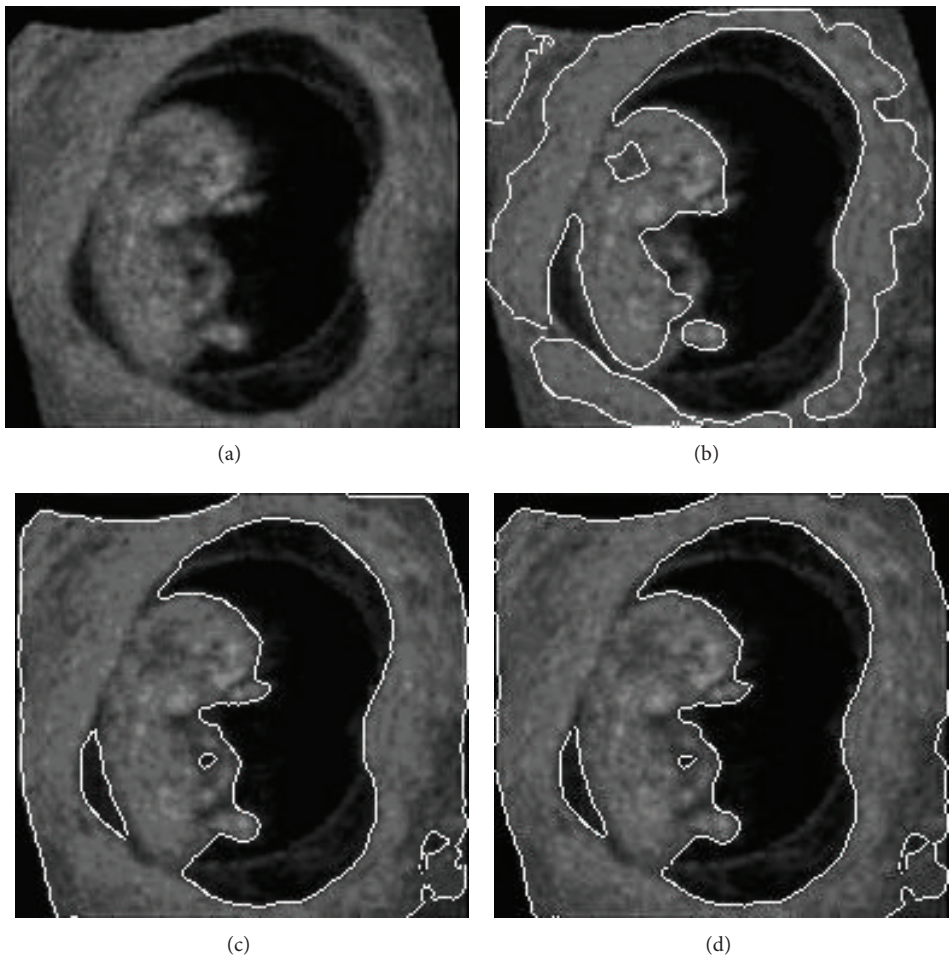

(a) (b) (c) (d)

Figure 3: Image for segmentation. (a) Original real ultrasound image. (b) The segmentation result using [36]. (c) The segmentation result using [37]. (d) The segmentation result using proposed model.

$$= \arg\min_{\vec{\omega}_1, u_1} \left\{ \int_\Omega \left(\beta_1 \left| \vec{\omega}_1 \right| dx\, dy + \alpha_1 \left(\frac{1}{2} \left(\frac{f}{u_1} \right)^2 + \log u_1 \right) + \frac{\mu_1}{2} \int_\Omega \left(\vec{\omega}_1 - \nabla u_1 - \vec{b}_1^{\,k} \right)^2 \right) \phi\, dx\, dy \right\}. \tag{7}$$

Fix $\vec{\omega}_1$ to solve u_1

$$u_1 = \arg\min_{u_1} \left\{ \int_\Omega \left(\alpha_1 \left(\frac{1}{2} \left(\frac{f}{u_1} \right)^2 + \log u_1 \right) + \frac{\mu_1}{2} \int_\Omega \left(\vec{\omega}_1 - \nabla u_1 - \vec{b}_1^{\,k} \right)^2 \right) \phi\, dx\, dy \right\}. \tag{8}$$

Using Euler-Lagrange equations we can get

$$\begin{aligned} \vec{b}^{k+1} &= \vec{b}^k + \nabla u_1^k - \vec{\omega}_1^k, \\ \alpha_1 \left(\frac{1}{u_1^k} - \frac{f^2}{\left(u_1^k\right)^3} \right) \phi - \mu_1 \nabla & \\ \cdot \left(\phi \left(\nabla u_1^{k+1} + \vec{b}^{\,k} - \vec{\omega}_1^k \right) \right) &= 0. \end{aligned} \tag{9}$$

Using implicit difference scheme to solve (9) we can get

$$\begin{aligned} u_1^{k+1} = & \left(\frac{1}{4\mu_1 + \left(\alpha_1 / \left(u_1^k\right)^2 \right)} \right) \\ & \times \left(\alpha_1 \left(\frac{f^2}{\left(u_1^k\right)^3} \right) + \mu_1 \left(u_{1(i+1,j)}^k + u_{1(i-1,j)}^k \right. \right. \\ & \left. + u_{1(i,j+1)}^k + u_{1(i,j-1)}^k \right. \\ & \left. \left. + \nabla \cdot \left(\vec{b}^{\,k} - \vec{\omega}_1^k \right) \right) \right). \end{aligned} \tag{10}$$

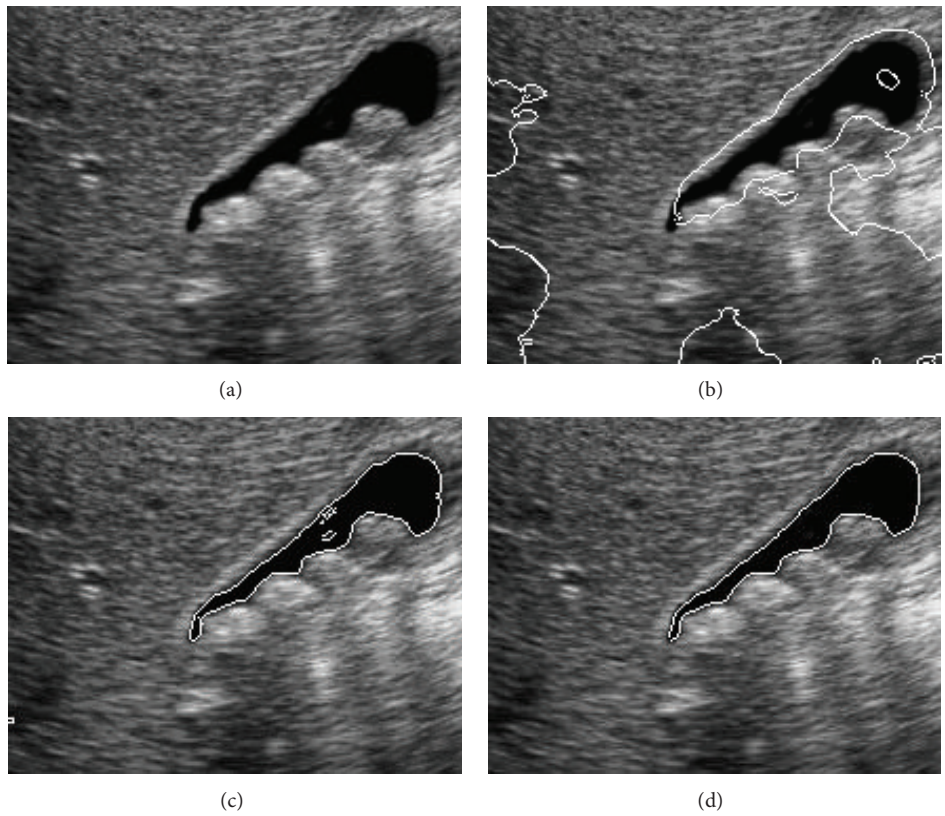

(a) (b) (c) (d)

Figure 4: Image for segmentation. (a) Original real ultrasound image. (b) The segmentation result using [36]. (c) The segmentation result using [37]. (d) The segmentation result using proposed model.

Fix u_1 to solve $\vec{\omega}_1$

$$\vec{\omega}_1 = \arg\min_{\vec{\omega}_1} \left\{ \int_\Omega \left(\beta_1 \varphi\left(\left|\vec{\omega}_1\right|\right) dx\, dy + \frac{\mu_1}{2} \int_\Omega \left(\vec{\omega}_1 - \nabla u_1 - \vec{b}_1^{\,k} \right)^2 \right) \phi\, dx\, dy \right\}. \tag{11}$$

The Euler-Lagrange equation of (11) is

$$\vec{\omega}_1^{k+1} = \nabla u_1^{k+1} + \vec{b}^{k+1} - \frac{\beta_1 \varphi'\left(\left|\vec{\omega}_1^{k}\right|\right)}{\mu_1} \frac{\vec{\omega}_1^{k+1}}{\left|\vec{\omega}_1^{k+1}\right|}. \tag{12}$$

We replace $\varphi(|\vec{\omega}_1|) = \gamma^2 \ln(1 + (|\vec{\omega}_1|^2/\gamma^2))$, then we can get the following equations.

Using generalized shrinkage formula [39] we can get

$$\vec{\omega}_1^{k+1} = \max\left(\left| \nabla u_1^{k+1} + \vec{b}^{k+1} \right| - \frac{\beta_1 \varphi'\left(\left|\vec{\omega}_1^{k}\right|\right)}{\mu_1}, 0 \right) \times \frac{\nabla u_1^{k+1} + \vec{b}^{k+1}}{\left| \nabla u_1^{k+1} + \vec{b}^{k+1} \right|}, \quad 0 \cdot \frac{0}{|0|} = 0, \tag{13}$$

where $\varphi'(|\vec{\omega}_1^{k}|) = |\vec{\omega}_1^{k}|/(1 + (|\vec{\omega}_1^{k}|^2/\gamma^2))$.

For solving u_2, the procedure is the same as solving u_1.

For solving (5), we also introduce auxiliary vector variable $\vec{v}$ and Bregman iterative parameter $\vec{d}$. Equation (5) can be transformed to the following:

$$\left(\phi^{k+1}, \vec{d}^{k+1}\right) = \arg\min_{\vec{d},\phi\in[0,1]} \left\{ \int_\Omega \left|\vec{v}\right| dx\, dy + \int_\Omega R\left(u_1, u_2\right) \phi\, dx\, dy + \frac{\lambda}{2} \int_\Omega \left(\vec{v} - \nabla\phi - \vec{d}^{k+1} \right)^2 dx\, dy \right\}, \tag{14}$$

where $\vec{d}^{k+1} = \vec{d}^{k} + \nabla\phi^{k} - \vec{v}^{k}$.

Alternative optimization of (14) results in the following equations.

Fix $\vec{v}$ to solve ϕ

$$\phi = \arg\min_{\phi\in[0,1]} \left\{ \int_\Omega \left(R\left(u_1, u_2\right) \phi\, dx\, dy + \frac{\lambda}{2} \left(\vec{v} - \nabla\phi - \vec{d}^{k+1} \right)^2 dx\, dy \right) \right\}. \tag{15}$$

By variational method, the Euler-Lagrange equation of (15) is

$$\lambda\left(\Delta\phi + \nabla\cdot\vec{d}^{k+1} - \nabla\cdot\vec{v}\right) - R\left(u_1, u_2\right) = 0. \tag{16}$$

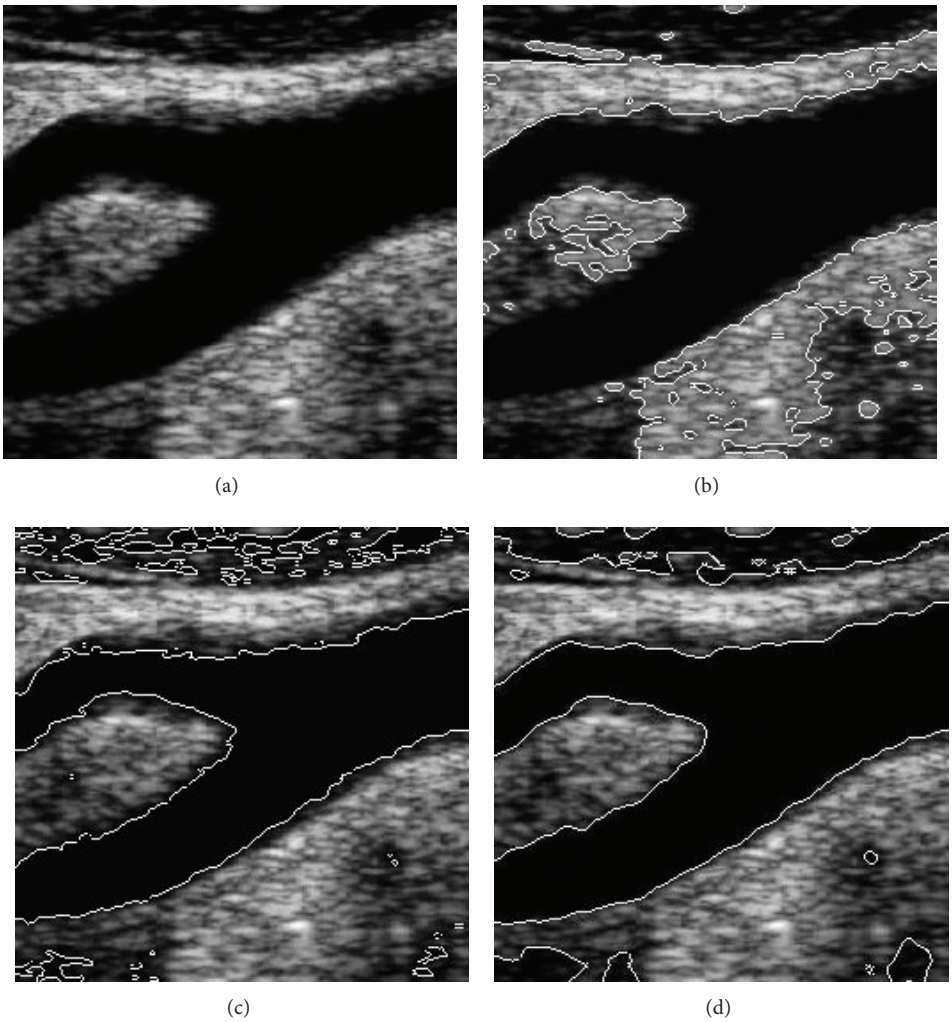

FIGURE 5: Image for segmentation. (a) Original real ultrasound image. (b) The segmentation result using [36]. (c) The segmentation result using [37]. (d) The segmentation result using proposed model.

Using gradient descent method, we can get ϕ:

$$\begin{aligned}\phi^{k+1} = &\left(\frac{1}{1+4\lambda t}\right)t \\ &\times\left(\lambda\left(\phi_{i,j-1}^{k}+\phi_{i,j+1}^{k}+\phi_{i-1,j}^{k}+\phi_{i+1,j}^{k}\right.\right. \\ &\left.\left.+\nabla\cdot\vec{d}^{k+1}-\nabla\cdot\vec{v}^{k}\right)-R\left(u_1,u_2\right)\right),\end{aligned} \tag{17}$$

and t is the time step and in the whole paper we set $t = 1$. Then we construct ϕ by projecting it on $[0, 1]$; that is,

$$\phi^{k+1} = \min\left(\max\left(\phi^{k+1},0\right),1\right). \tag{18}$$

Fix ϕ to solve $\vec{v}$

$$\vec{v} = \arg\min_{\vec{v}}\left\{\int_\Omega |\vec{v}|\,dx\,dy + \frac{\lambda}{2}\int_\Omega\left(\vec{v}-\nabla\phi-\vec{d}^{k+1}\right)^2 dx\,dy\right\}. \tag{19}$$

The Euler-Lagrange equation of (19) is

$$\vec{v}^{k+1} = \nabla\phi^{k+1} + \overrightarrow{d}^{k+1} - \frac{1}{\lambda}\frac{\vec{v}^{k+1}}{\left|\vec{v}^{k+1}\right|}. \tag{20}$$

$\vec{v}^{k+1}$ is also got using a generalized shrinkage formula [39]

$$\begin{aligned}\vec{v}^{k+1} = &\max\left(\left|\nabla\phi^{k+1}+\overrightarrow{d}^{k+1}\right|-\frac{1}{\lambda},0\right)\frac{\nabla\phi^{k+1}+\overrightarrow{d}^{k+1}}{\left|\nabla\phi^{k+1}+\overrightarrow{d}^{k+1}\right|}, \\ &0\cdot\frac{0}{|0|}=0.\end{aligned} \tag{21}$$

The initialization is also important; we set $u_1 = f$, $u_2 = 0$, $\overrightarrow{\omega}_1 = \overrightarrow{\omega}_2 = 0$, $\vec{g}_1 = \vec{g}_2 = 0$, $\vec{b}_1 = 0$, $\vec{b}_2 = 0$, $\vec{v} = 0$, $d = 0$, and $\phi = 0$.

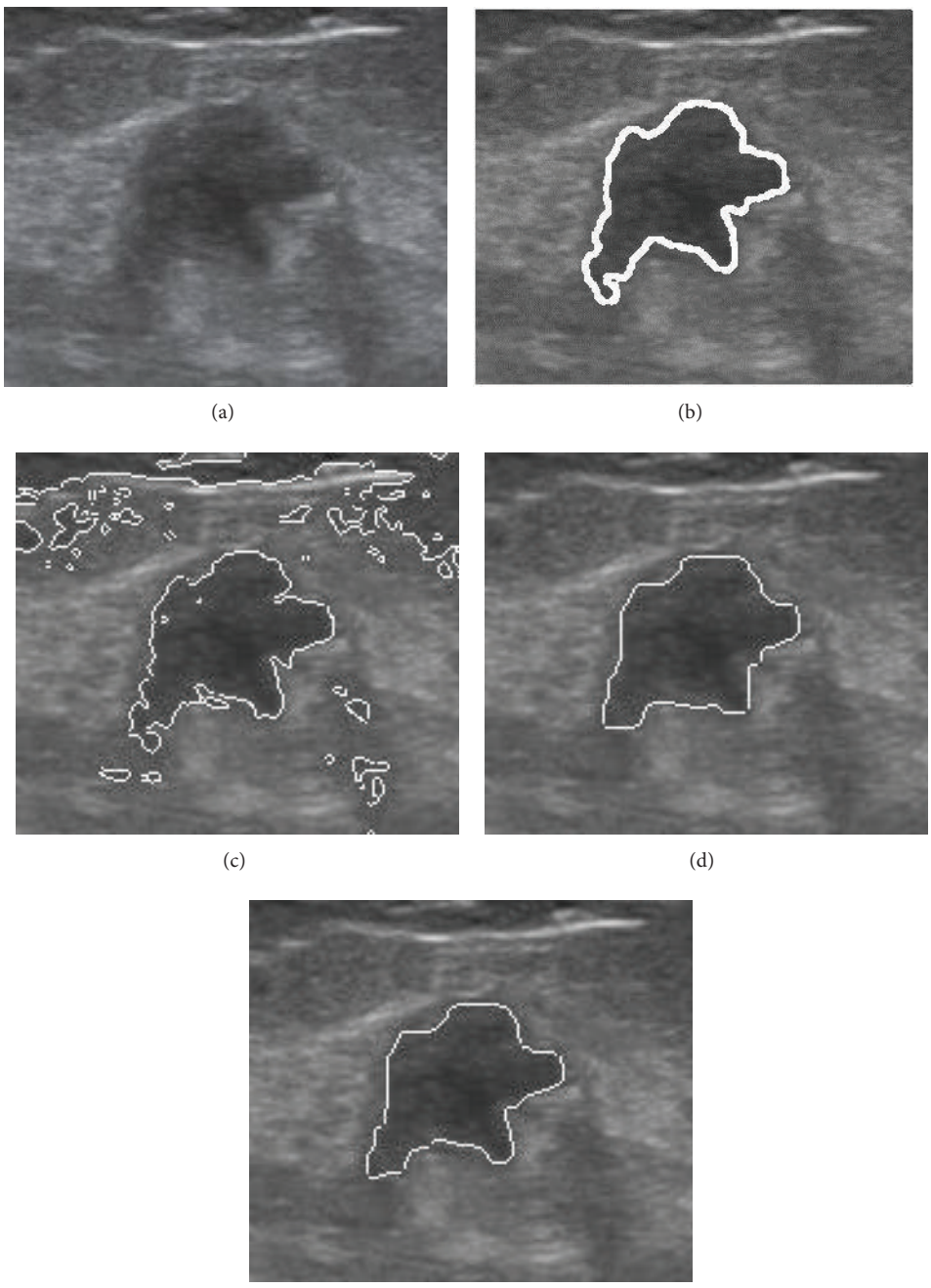

(a) (b) (c) (d) (e)

Figure 6: Image for segmentation. (a) Original real ultrasound image. (b) The ground truth of the segmentation. (c) The segmentation result using [36]. (d) The segmentation result using [37]. (e) The segmentation result using proposed model.

In the end of calculation, we set

$$\phi(x) = \begin{cases} 1 & \phi(x) \geq \text{th} \\ 0 & \phi(x) < \text{th}. \end{cases} \tag{22}$$

Thus the segmentation gets the real result. $\phi = 1$ corresponds to the segmentation target and $\phi = 0$ corresponds to the background. Our proposed new model is also globally convex due to $\phi \in [0, 1]$. That is to say, the position of ϕ does not need to be initialized.

4. Numerical Experiments

We test our method on a variety of synthetic images with multiplicative noise of Rayleigh distribution and real ultrasound images. We also compare the segmentation results of our method with the state-of-art methods in [36, 37]. For further comparison, we also give the quantitative analysis which includes the comparison of the results of our segmentation with the results derived from manual tracing.

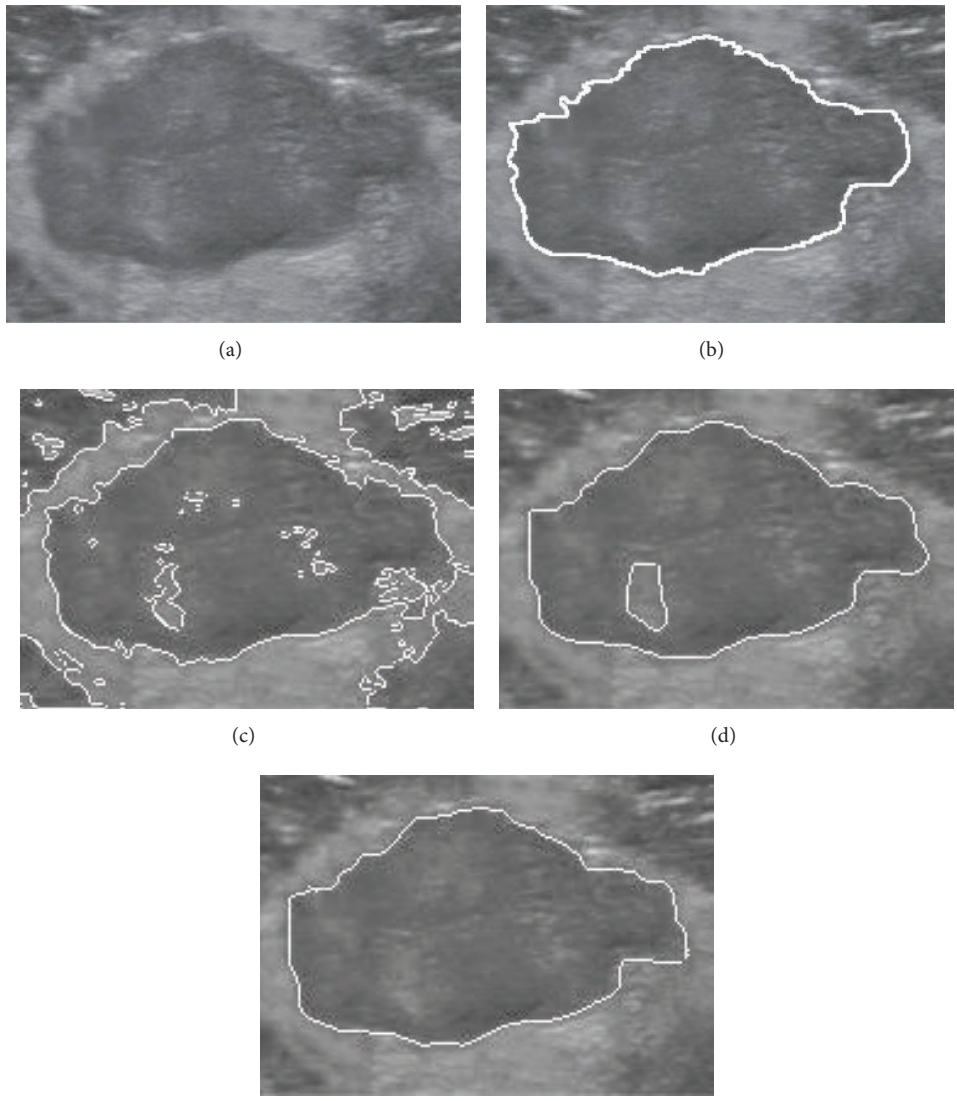

Figure 7: Image for segmentation. (a) Original real ultrasound image. (b) The ground truth of the segmentation. (c) The segmentation result using [36]. (d) The segmentation result using [37]. (e) The segmentation result using proposed model.

In all the experiments, we set $\gamma = 30$ in nonlinear function φ because this value is a stable one for noise removal. Figure 1 is a simple synthetic image corrupted by Rayleigh multiplicative noise and the variance is 0.08. Figure 1(a) is the origin synthetic noised image; Figures 1(b), 1(c), and 1(d) are the segmentation results using different methods. The parameters of our model referred to in the experiment are $\lambda = 200, \alpha_1 = 1, \alpha_2 = 1, \beta_1 = 0.5, \beta_2 = 0.5, \mu_1 = 0.1, \mu_2 = 0.1$, and th $= 0.006$ and iteration number is 20. Figures 1(c) and 1(d) are almost the same, but the segmentation of Figure 1(b) is not quite accurate and the corners and edges are not well segmented.

Figure 2 is the same image corrupted by larger noise with the same distribution as Figure 1 and the variance is 1. Figure 2(a) is the noisy image; Figures 2(b), 2(c), and 2(d) are the segmentation results using different methods. The parameters of our model referred to in the experiments are the same as in Figure 1, $\lambda = 200, \alpha_1 = 1, \alpha_2 = 1, \beta_1 = 0.5, \beta_2 = 0.5, \mu_1 = 0.1, \mu_2 = 0.1$, and th $= 0.006$, and iteration number is 20. From this experiment we can find that although there are some outliers and the edges are not well preserved, the method in [36] can still get proper segmentation result. But the method in [37] cannot get the segment result because of the large noise.

From Figure 2, we can find that although the image is very noisy, our proposed model still gets proper result and also captures the real edges. The last three experiments are tested on real ultrasound images. Figure 3 is an experiment on a real ultrasound image and the noise model is often considered as multiplicative noise with Rayleigh distribution. Figure 3(a) is the origin ultrasound image; Figures 3(b), 3(c), and 3(d) are the segmentation results using different

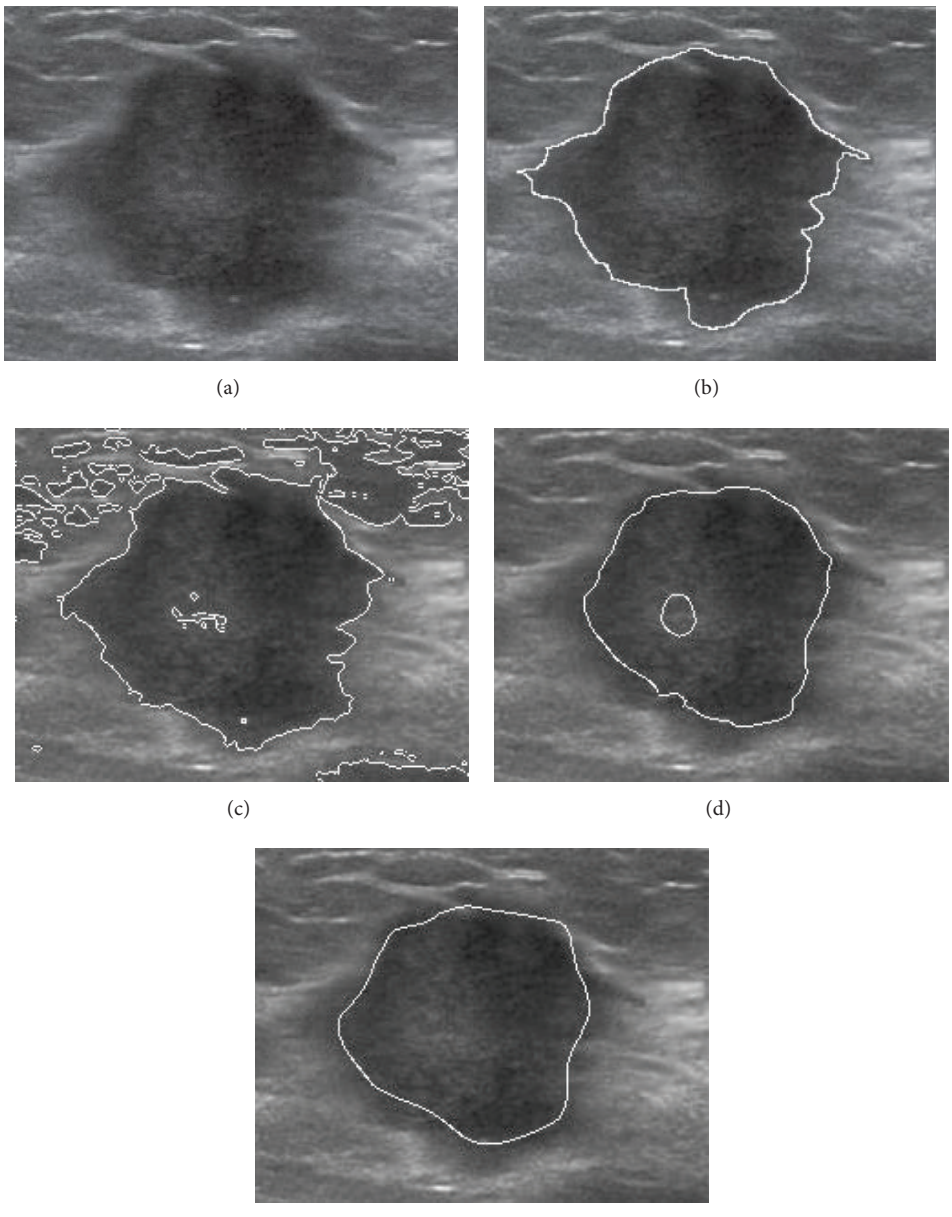

Figure 8: Image for segmentation. (a) Original real ultrasound image. (b) The ground truth of the segmentation. (c) The segmentation result using [36]. (d) The segmentation result using [37]. (e) The segmentation result using proposed model.

methods. The parameters of our model referred to in the experiment are $\lambda = 100$, $\alpha_1 = 1$, $\alpha_2 = 1$, $\beta_1 = 0.5$, $\beta_2 = 0.5$, $\mu_1 = 0.5$, $\mu_2 = 0.5$, and th = 0.04 and iteration number is 20.

Figure 4 is another real ultrasound image. Figure 4(a) is the origin ultrasound image; Figures 4(b), 4(c), and 4(d) are the segmentation results using different methods. The parameters of our model referred to in the experiment are $\lambda = 300$, $\alpha_1 = 0.5$, $\alpha_2 = 0.5$, $\beta_1 = 0.5$, $\beta_2 = 0.5$, $\mu_1 = 0.5$, $\mu_2 = 0.5$, and th = 0.02 and iteration number is 20.

Figure 5 is another real ultrasound image. Figure 5(a) is the origin ultrasound image; Figures 5(b), 5(c), and 5(d) are the segmentation results using different methods. The parameters of our model referred to in the experiment are $\lambda = 300$, $\alpha_1 = 0.5$, $\alpha_2 = 0.5$, $\beta_1 = 1$, $\beta_2 = 1$, $\mu_1 = 0.5$, $\mu_2 = 0.5$, and th = 0.06 and iteration number is 20.

From the results on real ultrasound images in Figures 3–5, we find that results using method in [36] cannot get good result because the model does not fit for multiplicative noise of Rayleigh distribution. The results using model in [37] get proper results but there are still some outliers because the model is proposed for Rayleigh distribution but it does not consider that the noise is also a multiplicative one.

For further explanation of the reliability of our proposed model, we compare our segmentation result with the gold standard which is represented by manual tracing by an expert observer. The operator manually traced the contour

of the area of interest which is time consuming. A set of 28 ultrasound images were manually traced by an expert. The manually traced contours were compared point-to-point to the corresponding active contour by the calculation of the Hausdorff distance [40]. From comparison between the manually and automatically traced contour, we find that they are in good agreement with error percentage of 2.1% ± 1.8%. The mean value of the Hausdorff distance between the manually and automatically traced contour is 1.2 pixels (range: 0.7–1.7 pixels).

Three examples of the automated segmentation versus the contour delineated by a radiologist are shown in Figures 6, 7, and 8 where the good correspondence can be appreciated. From the experiments, we also find that our results get better results than the other methods. All the experiments mentioned above show that our proposed method is very effective in ultrasound image segmentation.

5. Conclusion

In this paper, a new model active contour for ultrasound images is proposed. The model couples with multiplicative noise removal method for ultrasound image segmentation. For the easy implementation, the Split-Bregman method of the new model is also designed. The experiment results on various images show that the proposed method is good.

Conflict of Interests

The authors declare that there is no conflict of interests regarding the publication of this paper.

Acknowledgments

This work was supported by National Natural Science Foundation of China (no. 61305045, no. 61303079, and no. 61170106), National "Twelfth Five-Year" Development Plan of Science and Technology (no. 2013BAI01B03), Qingdao Science and Technology Development Project (no. 13-1-4-190-jch), and Natural Science Foundation of Shandong Province (no. ZR2010FQ030).

References

[1] V. Caselles, F. Catté, T. Coll, and F. Dibos, "A geometric model for active contours in image processing," *Numerische Mathematik*, vol. 66, no. 1, pp. 1–31, 1993.

[2] V. Caselles, R. Kimmel, and G. Sapiro, "Geodesic active contours," *International Journal of Computer Vision*, vol. 22, no. 1, pp. 61–79, 1997.

[3] M. Kass, A. Witkin, and D. Terzopoulos, "Snakes: active contour models," *International Journal of Computer Vision*, vol. 1, no. 4, pp. 321–331, 1988.

[4] S. Kichenassamy, A. Kumar, P. Olver, A. Tannenbaum, and A. Yezzi, "Gradient flows and geometric active contour models," in *Proceedings of the 5th International Conference on Computer Vision (ICCV '95)*, pp. 810–815, Cambridge, Mass, USA, June 1995.

[5] R. Malladi, J. A. Sethian, and B. C. Vemuri, "Topology-independent shape modeling scheme," in *Geometric Methods in Computer Vision II*, vol. 2031 of *Proceedings of SPIE*, pp. 246–258, San Diego, Calif, USA, July 1993.

[6] N. Paragios and R. Deriche, "Geodesic active contours for supervised texture segmentation," in *Proceedings of the IEEE Computer Society Conference on Computer Vision and Pattern Recognition (CVPR '99)*, pp. 699–706, Fort Collins, Colo, USA, June 1999.

[7] K. Siddiqi, Y. B. Lauzière, A. Tannenbaum, and S. W. Zucker, "Area and length minimizing flows for shape segmentation," *IEEE Transactions on Image Processing*, vol. 7, no. 3, pp. 433–443, 1998.

[8] C. Xu and J. L. Prince, "Snakes, shapes, and gradient vector flow," *IEEE Transactions on Image Processing*, vol. 7, no. 3, pp. 359–369, 1998.

[9] T. F. Chan and L. A. Vese, "Active contours without edges," *IEEE Transactions on Image Processing*, vol. 10, no. 2, pp. 266–277, 2001.

[10] Y. Chen, H. D. Tagare, S. Thiruvenkadam et al., "Using prior shapes in geometric active contours in a variational framework," *International Journal of Computer Vision*, vol. 50, no. 3, pp. 315–328, 2002.

[11] S. C. Zhu and A. Yuille, "Region competition: unifying Snakes, Region Growing, and Bayes/MDL for multiband image segmentation," *IEEE Transactions on Pattern Analysis and Machine Intelligence*, vol. 18, no. 9, pp. 884–900, 1996.

[12] N. Paragios and R. Deriche, "Geodesic active regions: a new framework to deal with frame partition problems in computer vision," *Journal of Visual Communication and Image Representation*, vol. 13, no. 1-2, pp. 249–268, 2002.

[13] M. Rousson and R. Deriche, "A variational framework for active and adaptative segmentation of vector valued images," in *Proceedings of the Workshop on Motion and Video Computing*, pp. 56–61, 2002.

[14] A. Herbulot, S. Jehan-Besson, M. Barlaud, and G. Aubert, "Shape gradient for multi-modal image segmentation using joint intensity distributions," in *International Workshop on Image Analysis for Multimedia Interactive Services*, 2004.

[15] S. Jehan-Besson, M. Barland, and G. Aubert, "DREAM^{2}S: deformable regions driven by an Eulerian accurate minimization method for image and video segmentation," *International Journal of Computer Vision*, vol. 53, no. 1, pp. 45–70, 2003.

[16] G. Aubert, M. Barlaud, O. Faugeras, and S. Jehan-Besson, "Image segmentation using active contours: calculus of variations or shape gradients?" *SIAM Journal on Applied Mathematics*, vol. 63, no. 6, pp. 2128–2154, 2003.

[17] B. Liu, H. D. Cheng, J. Huang, J. Tian, X. Tang, and J. Liu, "Probability density difference-based active contour for ultrasound image segmentation," *Pattern Recognition*, vol. 43, no. 6, pp. 2028–2042, 2010.

[18] J. Yuan, "Active contour driven by local divergence energies for ultrasound image segmentation," *IET Image Processing*, vol. 7, no. 3, pp. 252–259, 2013.

[19] Y. Pan, K. Feng, D. Yang, Y. K. Feng, and Y. Wang, "A medical image segmentation based on global variational level set," in *Proceedings of the ICME International Conference on Complex Medical Engineering (CME '13)*, pp. 429–432, Beijing, China, May 2013.

[20] X. Bresson, S. Esedoglu, P. Vandergheynst, J. P. Thiran, and S. Osher, "Fast global minimization of the active contour/snake

model," *Journal of Mathematical Imaging and Vision*, vol. 28, no. 2, pp. 151–167, 2007.

[21] T. F. Chan, S. Esedoglu, and M. Nikolova, "Algorithms for finding global minimizers of image segmentation and denoising models," *SIAM Journal on Applied Mathematics*, vol. 66, no. 5, pp. 1632–1648, 2006.

[22] T. Goldstein, X. Bresson, and S. Osher, "Geometric applications of the split Bregman method: segmentation and surface reconstruction," CAM Report 09-06, 2009.

[23] S. Simon, " Split bregman algorithm, douglas-rachford splitting and frame shrinkage," in *Scale Space and Variational Methods in Computer Vision*, vol. 5567 of *Lecture Notes in Computer Science*, pp. 464–476, Springer, 2009.

[24] X. Tai and C. Wu, "Augmented lagrangian method, dual methods and split bregman iteration for rof model," in *Proceedings of the 2nd International Conference on Scale Space and Variational Methods in Computer Vision (SSVM '09)*, vol. 5567 of *Lecture Notes in Computer Science*, pp. 502–513, Springer, Berlin Heidelberg, 2009.

[25] G. Wang, Z. Pan, J. Xu, Z. Zhang, C. Liu, and J. Ding, "Active contour model for images corrupted by multiplicative noise with rayleigh distribution," in *Proceedings of the IEEE 5th International Conference on Cybernetics and Intelligent Systems (CIS '11)*, pp. 124–127, Qingdao, China, September 2011.

[26] C. Wang, Z. Pan, Z. Zhang, W. Wei, and Q. Wang, "A general variational model for multiplicative noise removal and its split Bregman algorithm," in *Proceedings of the 3rd International Congress on Image and Signal Processing (CISP '10)*, vol. 2, pp. 571–577, Yantai, China, October 2010.

[27] D. Mumford and J. Shah, "Optimal approximations by piecewise smooth functions and associated variational problems," *Communications on Pure and Applied Mathematics*, vol. 42, no. 5, pp. 577–685, 1989.

[28] L. Rudin, P.-L. Lions, and S. Osher, "Multiplicative denoising and deblurring: theory and algorithms," in *Geometric Level Set Methods in Imaging, Vision, and Graphics*, pp. 103–119, Springer, 2003.

[29] G. Aubert and J. Aujol, "A variational approach to removing multiplicative noise," *SIAM Journal on Applied Mathematics*, vol. 68, no. 4, pp. 925–946, 2008.

[30] Y. Huang, M. K. Ng, and Y. Wen, "A new total variation method for multiplicative noise removal," *SIAM Journal on Imaging Sciences*, vol. 2, no. 1, pp. 20–40, 2009.

[31] S. Durand, J. Fadili, and M. Nikolova, "Multiplicative noise removal using L1 fidelity on frame coefficients," CMLA Report 08-40, 2008.

[32] S. Setzer, G. Steidl, and T. Teuber, "Deblurring Poissonian images by split Bregman techniques," *Journal of Visual Communication and Image Representation*, vol. 21, no. 3, pp. 193–199, 2010.

[33] J. Shi and S. Osher, "A nonlinear inverse scale space method for a convex multiplicative noise model," *SIAM Journal on Imaging Sciences*, vol. 1, no. 3, pp. 294–321, 2008.

[34] J. Shen, "Webers law and weberized TV restoration," CMLA Report 02-20, 2002.

[35] L. Denis, F. Tupin, J. Darbon, and M. Sigelle, "SAR image regularization with fast approximate discrete minimization," *IEEE Transactions on Image Processing*, vol. 18, no. 7, pp. 1588–1600, 2009.

[36] M. Le and A. Vese, "Additive & multiplicative piecewise-smooth segmentation models in a functional minimization approach," in *Interpolation Theory and Applications: A Conference in Honor of Michael Cwikel, Miami, Florida*, L. de Carli and M. Milman, Eds., vol. 445 of *Comtemporay Mathematics*, pp. 207–223, 2007.

[37] A. Sarti, C. Corsi, E. Mazzini, and C. Lamberti, "Maximum likelihood segmentation of ultrasound images with rayleigh distribution," *IEEE Transactions on Ultrasonics, Ferroelectrics, and Frequency Control*, vol. 52, no. 6, pp. 947–960, 2005.

[38] L. A. Vese and T. F. Chan, "A multiphase level set framework for image segmentation using the Mumford and Shah model," *International Journal of Computer Vision*, vol. 50, no. 3, pp. 271–293, 2002.

[39] J. Yang, W. Yin, Y. Zhang, and Y. Wang, "A fast algorithm for edge-preserving variational multichannel image restoration," *SIAM Journal on Imaging Sciences*, vol. 2, no. 2, pp. 569–592, 2009.

[40] E. Belogay, C. Cabrelli, U. Molter, and R. Shonkwiler, "Calculating the Hausdorff distance between curves," *Information Processing Letters*, vol. 64, no. 1, pp. 17–22, 1997.